

# LUNAR OBSERVER LASER ALTIMETER OBSERVATIONS FOR LUNAR BASE SITE SELECTION

N 93 - 17437

James B. Garvin and Jack L. Bufton

NASA Goddard Space Flight Center  
Greenbelt MD 20771

*One of the critical datasets for optimal selection of future lunar landing sites is local- to regional-scale topography. Lunar base site selection will require such data for both engineering and scientific operations purposes. The Lunar Geoscience Orbiter or Lunar Observer is the ideal precursory science mission from which to obtain this required information. We suggest that a simple laser altimeter instrument could be employed to measure local-scale slopes, heights, and depths of lunar surface features important to lunar base planning and design. For this reason, we have designed and are currently constructing a breadboard of a Lunar Observer Laser Altimeter (LOLA) instrument capable of acquiring contiguous-footprint topographic profiles with both 30-m and 300-m along-track resolution. This instrument meets all the severe weight, power, size, and data rate limitations imposed by Observer-class spacecraft. In addition, LOLA would be capable of measuring the within-footprint vertical roughness of the lunar surface, and the 1.06- $\mu\text{m}$  relative surface reflectivity at normal incidence. We have used airborne laser altimeter data for a few representative lunar analog landforms to simulate and analyze LOLA performance in a 100-km lunar orbit. We demonstrate that this system in its highest resolution mode (30-m diameter footprints) would quantify the topography of all but the very smallest lunar landforms. At its global mapping resolution (300-m diameter footprints), LOLA would establish the topographic context for lunar landing site selection by providing the basis for constructing a 1-2 km spatial resolution global, geodetic topographic grid that would contain a high density of observations (e.g., ~1000 observations per each 1° by 1° cell at the lunar equator). The high spatial and vertical resolution measurements made with a LOLA-class instrument on a precursory Lunar Observer would be highly synergistic with high-resolution imaging datasets, and will allow for direct quantification of critical slopes, heights, and depths of features visible in images of potential lunar base sites.*

## INTRODUCTION AND BACKGROUND

Many of the scientific and engineering issues associated with the selection of potential lunar base sites or any future lunar landing sites require a detailed knowledge of local and regional-scale topography (Wilhelms, 1985). Prior to the human Apollo missions to the Moon, extremely high resolution Lunar Orbiter photographs were acquired in stereo in order to assess the local topography and geology of candidate human landing sites. Such data were especially critical for those missions involving the Lunar Rover vehicle (i.e., Apollo 15-17), as the rover could only negotiate terrain with slopes less than several degrees. In an important study of local-scale lunar roughness and slopes, H. J. Moore et al. (unpublished data, 1969) outlined the kinds of local terrain data necessary for a realistic and accurate assessment of potential implications of lunar topography for human operations. Moore et al. (1980) used a combination of orbital stereo photography, bistatic radar, and Earth-based radar to assess lunar RMS roughnesses indirectly, and then compared the independent results with reasonable agreement. However, a direct means of globally measuring local lunar surface roughness and slopes was technologically not feasible in the early 1970s.

The Apollo Laser Altimeter (flown on Apollo 15-17) obtained surface elevation data for 3-m footprints at 1-2 m vertical accuracy; however, the limited lifetime and low pulse repetition frequency (PRF) of the ruby laser allowed only one range measurement for every 30 km along the suborbital track of the Command Service Module (Kaula et al., 1974). Thus, the

circumlunar topographic profiles that were acquired have a very low spatial resolution and can only be used to measure slopes on baselines of 60 km and longer.

Lunar Topographic Orthophotomaps (LTOs) have been constructed for many areas on the Moon, and these high-quality stereophotogrammetric topographic data have effective spatial resolutions as good as a few hundred meters with ~10-m relief contours (Ravine and Grieve, 1986). However, the LTO data do not form a global, high-integrity, topographic model for the entire lunar surface, or even for a large fraction thereof.

Orbital radar techniques during the Apollo era (i.e., the ALSE experiment flown on Apollo 17) obtained kilometer-resolution profiles of lunar topography (Moore et al., 1980; Sharpton and Head, 1982), as have Earth-based radar techniques. A global lunar topographic model with 2-5-km grid cells (spatial resolution) could be obtained using existing narrow-beam radar altimeter techniques (Phillips, 1986) from a lunar polar orbiter. Such a dataset would be invaluable for establishing an accurate control net relevant to lunar landings and lunar base site selection, as well as for long-wavelength geophysical studies and for determining regional-scale topographic characteristics of all major terrain types on the Moon. Without resorting to very large antennae, high-frequency radar altimeter designs such as those currently under development for the Earth Observing System, local-scale high-resolution (<0.5 km) topography of the Moon can only be directly assessed from high-repetition-rate orbital laser altimetry. Technological breakthroughs in laser lifetime now permit pulsed laser altimeter instruments to operate continuously for a complete



rapid than the Apollo Laser Altimeter. Assuming a nominal 100-km orbital altitude, the 30-m-diameter footprint profiles will be separated across track by ~2 km at the lunar equator, but will rapidly converge at increasing latitudes. These high-resolution profiles would be circumlunar in their coverage. In order to adequately sample the regional topography of the Moon, a second spatial resolution mode is recommended for a LOLA instrument. Orbital simulations suggest that 300-m-diameter footprints could easily be achieved; this spatial resolution would diminish the effect of coverage gaps at the lunar equator by an order of magnitude and permit rapid acquisition of a dataset suitable for gridding at a 1-2-km level. The 300-m-diameter footprints could be contiguous or, if desirable, they could be overlapped by up to 50% to reduce sampling biases. If the LOLA instrument could continuously measure the lunar topography in this lower resolution mode for a period of ~1 year, nearly 60% of the lunar surface would be sampled, and a subkilometer topographic grid could be constructed.

Vertical resolution for either the 30-m or 300-m modes on LOLA is dictated by laser pulsewidth (i.e., the duration in time of the central part of the transmitted laser pulse), time-interval counter (TIC) resolution, and pointing control and knowledge. Table 1 summarizes the baseline design parameters that have been chosen for LOLA. The 3-nsec laser pulsewidth (full width at half maximum) coupled with a 1-nsec TIC resolution provides 15-cm vertical resolution under ideal conditions. This is because there are ~6.67 nsec per meter of relief (due to the speed of light), and the narrower in time a laser pulse can be made, the easier it is to track after it interacts with a random surface (and is naturally spread in time). The TIC is a very fast counter that is activated when each laser pulse is transmitted, and stopped once some critical threshold level on the backscattered laser pulse is detected. A 1-nsec TIC resolution ensures timing precision to 15 cm. However, final vertical accuracies will depend on local surface slopes, within footprint roughness, pointing knowledge, and orbit determination. Aircraft laser altimeter systems capable of this level of performance are now operating out of NASA's Goddard Space Flight Center.

Tables 1-4 summarize those design and performance parameters for LOLA that we feel should provide maximum information with respect to lunar geoscience objectives and lunar base site selection. Figure 1 illustrates the inherent simplicity of the LOLA design in a functional block diagram. It should be emphasized that LOLA requires no onboard signal analysis or complex pulse averaging to make a range measurement. In fact, every single transmitted laser pulse would result in a unique, independent range, and relative reflectivity measurement. The LOLA design under development as part of NASA's Planetary Instrument Definition and Development Program (PIDDP) provides three types of data relevant to lunar surface properties for each and every footprint: range (elevation), 1.06- $\mu$ m relative reflectivity at normal incidence, and vertical RMS roughness (i.e., a measure of the total dynamic range of relief within each 30-m or 300-m footprint). The 1.06- $\mu$ m reflectivity within 300-m-diameter footprints would be synergistic with Visual Infrared Mapping Spectrometer (VIMS) observations of lunar surface mineralogy (Phillips, 1986). The 30-m and 300-m LOLA footprint RMS vertical roughness would allow for after-the-fact retracking of LOLA topographic observations (in rougher terrains), and would be complementary to active or passive microwave observations of lunar roughness (e.g., from a multichannel microwave radiometer on LGO, or from Earth-based radar observations). Local

TABLE 1. LOLA laser altimeter instrument parameters.

<i>Laser Transmitter</i>	
Laser Type	Diode-pumped, Q-switched Nd:YAG
Wavelength	1.06 $\mu$ m
Pulse Energy	2 mJoule
Pulsewidth	3 nsec FWHM
Repetition rate	10 Hz or 50 Hz
Divergence	0.3 or 3.0 mrad
Lifetime	10 <sup>9</sup> shots minimum (3 yr @ 10 Hz)
<i>Altimeter Receiver</i>	
Telescope Type	f/1 diamond-turned aluminum parabola
Telescope Diameter	25 cm
Optical Filter	2 nm bandpass
Detector Type	Silicon Avalanche Photodiode
Quantum Efficiency	40%
Sensitivity	1 nWatt
Time-Interval Counter	1-nsec resolution
Waveform Digitizer	Pulse width, power, and energy

TABLE 2. LOLA payload parameters.

Size	25 cm $\times$ 25 cm $\times$ 35 cm (0.022 m <sup>3</sup> )	
Weight	15 kg (33 lb)	
Operating Modes	Standard-rate (10Hz)	Burst (50Hz)
Power	10 W	15 W
Data Rate	1 kbps	3.5 kbps
Duty Cycle	Continuous	
Thermal	Passive control with insulation and radiators	
Mounting	Spacecraft bus	

TABLE 3. LOLA performance in 100-km lunar orbit.

Sensor Footprint	30 or 300 m
Along-Track Data Interval	Contiguous coverage
Vertical Resolution	15 cm
Vertical Accuracy	Submeter
Surface Roughness Resolution	Submeter
Surface Albedo Resolution	1% for 1.06 $\mu$ m backscatter

TABLE 4. Typical standard deviations (SD) of topography within 30-m-diameter footprints (LOLA scale) for analog landforms relevant to planetary surfaces.

Target	Landform Type (and subtype)	SD Topography (m)
Meteor Crater	Impact crater	1-26
	Steepest inner wall	12-26
	Near-rim ejecta	2-6
	Rim	2-7.5
	Distal ejecta	0.2-2
	Floor	1-2
	Edge of ejecta	4-6
Grand Canyon	Erosional canyon (fluvial/tectonic)	1-72
	Walls of deepest canyon	60-72
	Typical canyon walls	35-60
	Canyon floors	3-8
Iceland lavas	Lava channel (pahoehoe)	0.2-2.0
	Flow margins	0.9-2.0
	Typical flow interior surface	0.2-0.3
	Roughest flow surface	0.3-0.5
Water*	Atlantic Ocean (Iceland bay)	0.15-0.3

\* Control surface for reference with respect to 30-m baseline roughness.

topographic gradients on baselines as short as 60 m could be computed directly from LOLA profiles.

In order to obtain these complementary global datasets using a LOLA instrument in a 100-km lunar orbit, the fundamental engineering challenges are primarily related to the laser transmitter and receiver. There must be adequate "link margin" for the LOLA laser to obtain range observations during both lunar night and day, and for surfaces with a diverse range of infrared albedos and local height variations. "Link margin" is analogous to signal-to-noise ratio (SNR) and is simply a measure of the degree of confidence that an adequate number of photons above background level will be received and detected by the instrument in order for a useful range measurement to be achieved. The laser transmitter pulse energy and detector sensitivity must be adequately flexible to respond to a range of operational extremes. Our computations suggest that the instrument parameters listed in Table 1 are sufficient to meet the anticipated range of surface albedos and background 1.06- $\mu\text{m}$  illumination conditions (e.g., solar). The experience with the Apollo Lunar Laser Altimeter provides adequate data to make this assessment (*Kaula et al.*, 1974; *Moore et al.*, 1980). Less is known about what to expect with respect to the spectrum of 30-300-m scale height variations and local slopes (*Moore et al.*, unpublished data, 1969).

The primary engineering challenge associated with lunar orbital laser altimetry concerns development of a space-qualified laser using modern, all-solid-state technology. In addition, a compact, low-power laser backscatter waveform digitizer must be validated for operations in lunar orbit. Waveform digitizers record the shapes of input signals in terms of amplitude as a function of time and are electronically complex, but they have been space qualified for use in microwave instruments. Recent breakthroughs in all-solid-state laser oscillators (*Byer*, 1988) now permit high pulse-repetition-rate laser operations for at least 1 billion pulses, and perhaps up to 3 billion. This is because the traditional flashlamp method of pumping the Nd:YAG (a material that has replaced ruby) laser rod has been replaced with a highly efficient array of laser diodes. Flashlamps have traditionally been required to inject enough optical energy into the laser material for it to lase. Longer-lived arrays of laser diodes can now serve this purpose. The so-called diode-pumped Nd:YAG laser oscillator offers the required performance characteristics (e.g., 50-Hz repetition rate, short pulse, low power and mass) for spaceborne operation. Efficient, low-power diode-pumped Nd:YAG lasers have recently been space qualified by McDonnell Douglas for laser tracking purposes (*Long et al.*, 1989). The lunar environment with its total absence of an atmosphere is ideal for orbital laser altimeter operations. Figure 2 is a photograph of the LOLA breadboard that illustrates its compact form. Refer to Table 2 for specific payload parameters.

Airborne simulations of the LOLA breadboard are expected to occur during the 1990-1991 timeframe in order to facilitate development of a full-instrument prototype. Simulations of LOLA performance using degraded airborne laser altimeter profiles for lunar analog terrains are currently underway to explore potential requirements for lunar base site selection and activities. Examples from these datasets will be discussed in the next section.

## LOLA SIMULATIONS

A high-altitude airborne laser altimeter instrument is currently in operation at NASA's Goddard Space Flight Center (*Buften and Garvin*, 1987). This instrument is configured in a NASA Wallops

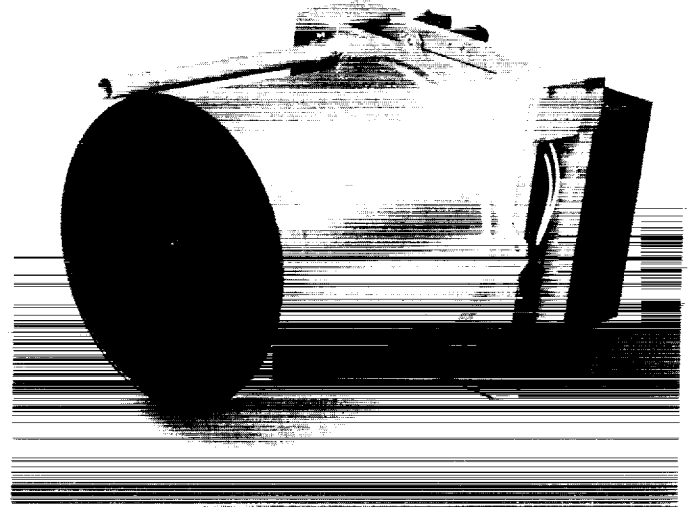


Fig. 2. Photograph of the LOLA breadboard with bar for scale. The instrument is similar in size to the Thermal Emission Spectrometer that is to be flown to Mars on the Mars Observer in 1992. The laser transmitter and receiver electronics are located in the rectangular box that is affixed atop the telescope. The laser beam is guided by the small tube parallel to the telescope.

Flight Facility T-39 Sabreliner jet aircraft, and is capable of obtaining laser profiles from altitudes as high as 11 km, or as low as 1-2 km above terrain. This airborne laser altimeter instrument has been used to acquire 3-10-m spatial resolution topographic profiles with submeter vertical precision for a variety of volcanic, erosional, and impact targets in the western and southwestern United States. Another currently operational instrument (at NASA's Wallops Flight Facility) is the Airborne Oceanographic Lidar (AOL), which has a low-altitude laser altimeter mode with 25-30-cm-diameter footprints and  $\sim 30$ -cm vertical resolution (*Hoge et al.*, 1984). We present and discuss the implications of profiles obtained from these airborne systems that have been degraded to LOLA spatial and vertical resolution using straightforward offset-averaging techniques. Specifically, for each n-point window (where "window" refers to the width in meters of a profile subsection), the mean and standard deviation of the topography is computed (i.e.,  $n = 10$  to 100). The window is then translated n points, and the process is repeated. The standard deviation is a good estimate of the LOLA vertical roughness parameter, while the n-point mean is a reasonable indicator of the 30-m footprint topographic measurement. Table 4 summarizes the range of 30-m-diameter footprint topographic standard deviations observed for a diverse set of lunar analog surfaces.

While most lunar landforms within the younger maria are relatively pristine, micrometeorite bombardment over the past 2-3 b.y. (AE) has resulted in the generation of a regolith layer that mantles the original topography, especially the lunar lava flows. The thickness of this regolith mantle varies from meters to hundreds of meters (*Wilhelms*, 1987). In spite of this lunar erosion effect, aspects of the morphology of such basic lunar landforms as craters, rilles, lava flow fronts, and hummocky ejecta have been preserved (*Wilhelms*, 1987); thus the LOLA simulations for the lunar analog landforms are relevant, even if they represent

endmember scenarios. Lunar base site selection is likely to be a very complex process involving many tradeoffs, and base location in proximity to youthful lunar volcanic or impact deposits is certainly worth consideration. What follows is a brief description of a set of LOLA simulation profiles for representative lunar analog landforms, with comments relevant to lunar base site selection and eventual operations.

### Meteor Crater (Barringer), Northern Arizona

One of the most youthful impact craters on Earth is Meteor (Barringer) Crater, located in north-central Arizona (Fig. 3a). This well-studied impact crater is  $\sim 1.2$  km in average diameter, and formed as a result of a  $\sim 20$ -megaton hypervelocity impact of an iron meteorite about 49,000 years ago (Schoemaker, 1987). Figure 4 is a LOLA resolution laser altimeter profile across the center of the crater from northwest to southeast, with the standard deviation of the 30-m-scale topography shown as individual dots. A full-resolution (3-m-diameter footprints) profile is illustrated in Fig. 3b for comparison. Figure 5 is a Lunar Orbiter III photograph of a simple impact crater 520 m in diameter in Oceanus Procellarum, which is located about 16 km from the Apollo 12 landing site (Cintala *et al.*, 1982) and is similar to Meteor Crater, in part due to its freshness. One can observe the 2-30-m-diameter impact-generated blocks within the ejecta blanket of this crater. As part of a study of excavation efficiency of the cratering process on the Moon, Cintala *et al.* (1982)

measured the size distribution of all the blocks larger than 1.5 m in diameter around this crater as a function of distance from the crater center. Figure 6 displays the size distribution of ejecta blocks for the entire continuous ejecta blanket and indicates the significance of meter-scale roughness elements such as blocks at local scales, even on the relatively smooth lunar maria. The simulated LOLA topographic profile in Fig. 4 illustrates the 2-6-m vertical roughness (standard deviation of topography) that occurs in the Meteor Crater near-rim ejecta blanket. It is also possible to observe the large range of topographic variance associated with the inner crater walls, which are known to have local slopes as high as  $41^\circ$  (computed from Fig. 3b; see also Table 4). The inner wall slopes of the lunar crater shown in Fig. 5 are approximately as steep as those in Meteor Crater on the basis of shadow measurements. Such inner crater walls have over 25 m of vertical roughness in several instances (see Fig. 4). Although terrestrial erosion processes have filled in the floor of Meteor Crater beyond the extent typical of cratering-related slumping effects, most of the critical morphologic elements are preserved, including the discontinuous ejecta blanket. Thus it is possible to learn about the types of local topography and roughness that are likely to be common in association with the ubiquitous simple impact craters that frequently occur even on the smooth mare. If lunar base site selection is to follow the safety criteria imposed during the first few Apollo landings, then surfaces like those illustrated in Fig. 5 are likely to be commonplace, and the scales of roughness observed at Meteor Crater (Fig. 3a) will be relevant for base construction and local operations.

ORIGINAL PAGE  
BLACK AND WHITE PHOTOGRAPH

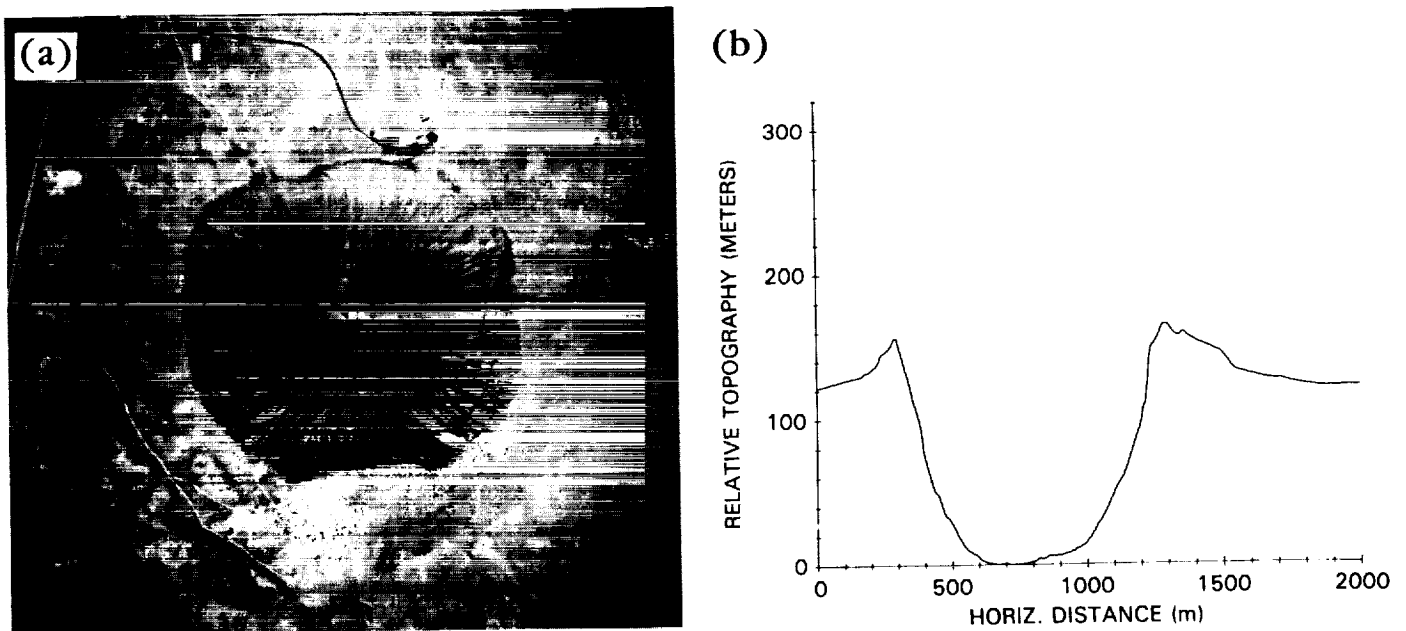


Fig. 3. (a) Vertical airphoto of Meteor Crater acquired in 1967 with a large format metric camera. Resolution is  $\sim 1$  m. The frame shows the Crater Museum at the top (north), as well as the full extent of the preserved ejecta blanket (out to about 2 crater radii). The rim crest diameter of Meteor Crater averages 1.2 km, and the average depth is 165 m. (b) Airborne laser altimeter profile of Meteor Crater from northwest to southeast. Horizontal sampling interval is  $\sim 3$  m, and vertical precision is submeter. This profile crosses the impact crater center and illustrates the asymmetry of the ejecta blanket (profile acquired in October 1986).

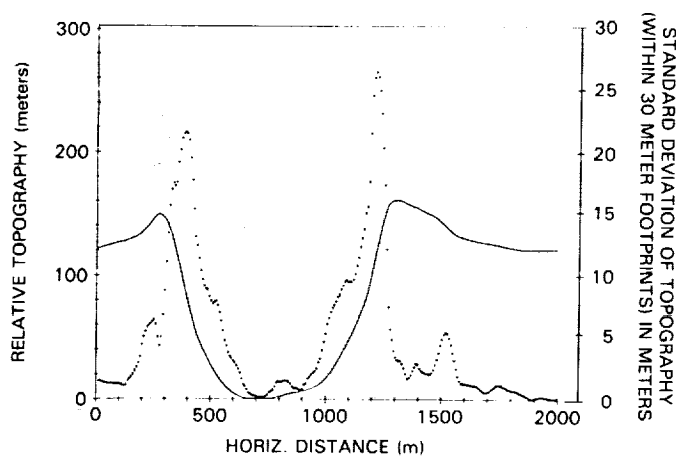


Fig. 4. Spatially degraded version of the profile shown in Fig. 3b using the sliding window offset technique described in the text. The horizontal sampling interval is 30 m. The superimposed dots are a measure of the standard deviation of topography within each 30-m footprint (see right axis). Note the edge effects displayed by this parameter, especially for the locally steep inner walls of the crater (see Table 4). The standard deviation parameter is a good estimate of the LOLA vertical roughness parameter to be derived from the shape of the backscattered laser waveform.

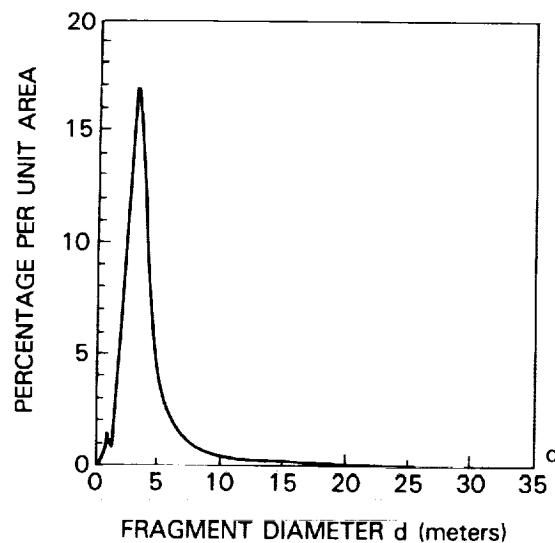


Fig. 6. Size frequency distribution for ejecta blocks within continuous ejecta deposit for the crater shown in Fig. 5 (Cintala et al., 1982). In combination with orbital imagery, LOLA profile data would permit assessment of local hazards (such as 20-30-m-diameter blocks) associated with commonplace fresh impact craters. Note that only blocks 1.5 m and larger were included in the study due to orbital image resolution constraints (Lunar Orbiter III).

ORIGINAL PAGE  
BLACK AND WHITE PHOTOGRAPH

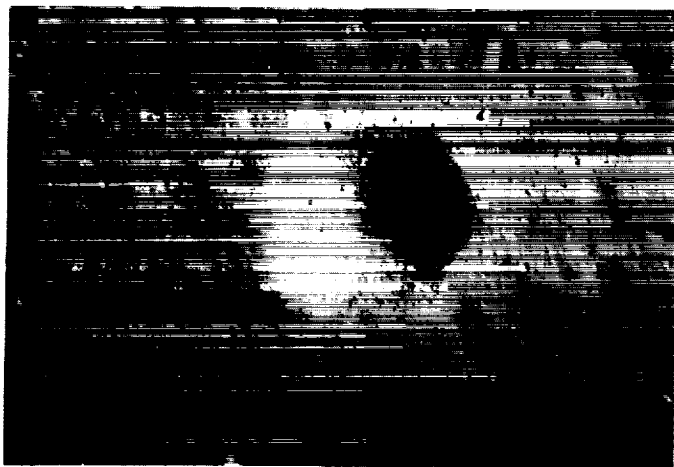


Fig. 5. Lunar Orbiter III image of a 520-m-diameter crater near the Apollo 12 site (Oceanus Procellarum) in a region of the maria with thin regolith (~7 m). Observe the 2-30-m-diameter ejecta blocks scattered around the rim of this simple, fresh impact crater.

### Grand Canyon, Northern Arizona

As an example of the extremes of lunar topography, LOLA resolution topographic profiles of the interior of the Grand Canyon (including the Colorado River, Fig. 7a) have been examined. While erosional topography associated with fluvial processes acting on a variety of sedimentary, igneous, and metamorphic lithologies is not likely to exist on the Moon, the deepest lunar rilles and most youthful complex impact craters are

known to have steep topography (Wilhelms, 1987). Thus we use the severe local slopes associated with the southern Grand Canyon as a means of demonstrating a worst-case scenario for the Moon. Figure 7b is a 3-m spatial resolution profile from south to north across the southern rim of the Grand Canyon; the deepest point is the Colorado River (at right). Figure 8 is a LOLA resolution profile with superimposed vertical roughness shown by individual dots, as with Meteor Crater above. Up to 75 m of vertical relief is observed within the 30-m-diameter simulated LOLA footprints (Table 4). Deep lunar sinuous rilles, which may have formed by thermal erosion from turbulent, low-viscosity lavas, could have over 50 m of relief within each 30-m LOLA footprint. It is clear from the LOLA simulation that high spatial and vertical resolution orbital laser altimetry will permit adequate sampling of the local topography, slopes, and roughnesses of many types of lunar surfaces, however extreme or subtle. With respect to lunar base site selection, the location of a base in close proximity to deep rilles may offer advantages with respect to possible resource development, as the walls of such landforms often display exposed volcanic units (e.g., as at Apollo 15 near Hadley Rille), which could provide accessible materials for various purposes. Knowledge of the extremity of local topography and slopes is certainly a requirement to ensure that the potential base site is not within possible slump-failure zones, which might be associated with the areas adjacent to the walls of such rilles.

While meter-resolution stereophotogrammetric techniques have been successfully employed for measuring local slopes (e.g., H.J. Moore et al., unpublished data, 1969; lunar topographic photomaps), it is virtually impossible to establish geodetic control with such methods beyond the field of view of individual stereo pairs; orbital altimetry is usually necessary to provide the required

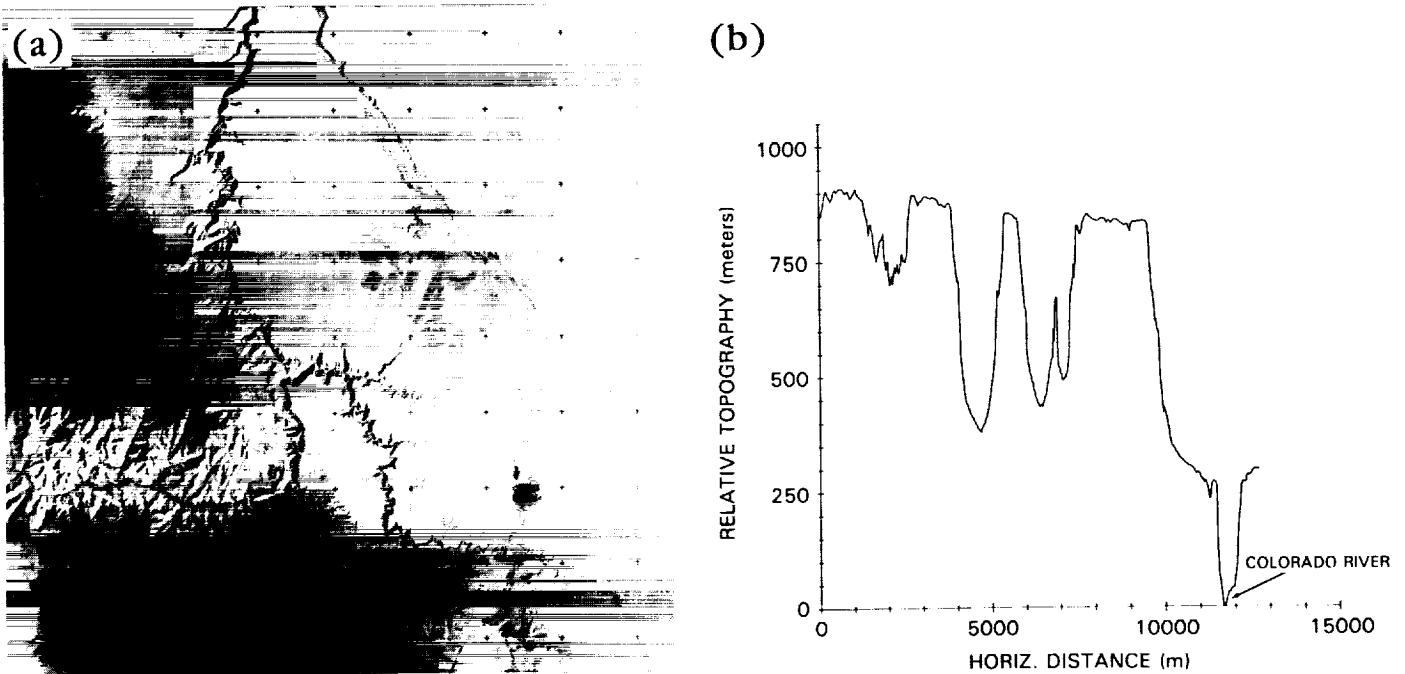


Fig. 7. (a) Landsat MSS orbital image of the Grand Canyon region of northern Arizona acquired in autumn of 1980 at a resolution of 80 m. The profile shown in (b) extends from south to north and traverses the section of the canyon illustrated in the middle left of this image (from the south rim to the Colorado River). This image shows the east-west and other branches of the Grand Canyon, as well as the heavily forested area south of the canyon (dark region in lower part of image). (b) Airborne laser altimeter profile of the southern part of the Grand Canyon (from south to north in Arizona). The deepest point (at right) is the Colorado River. As in Fig. 3b, the horizontal sampling interval is  $\sim 3$  m (profile acquired in October 1986).

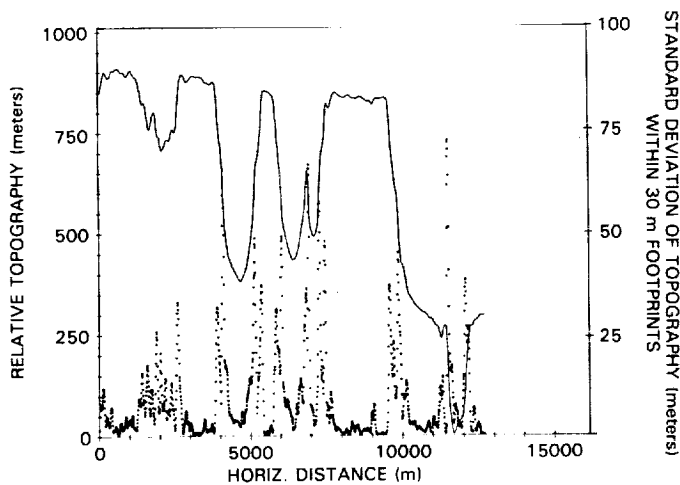
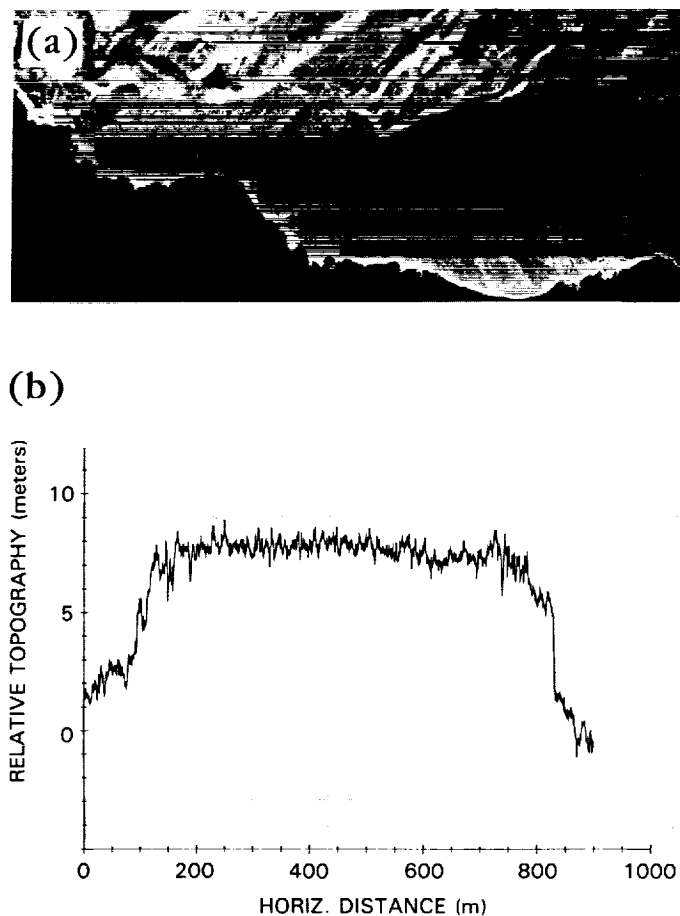


Fig. 8. As in Fig. 4, simulated LOLA profile for the Grand Canyon derived from the data shown in Fig. 7b, with superimposed 30-m scale topographic variance parameter (see righthand side vertical axis for scale) shown as dots.

longer-wavelength control. In addition, stereophotogrammetric methods are somewhat operator dependent (subjective), and time consuming. Our approach has been to design an orbital altimeter system capable of both tasks, and the LOLA simulations of the Grand Canyon and Meteor Crater discussed above provide some justification of this claim.

#### Lava Channel, Southwest Iceland

As a final example, an  $\sim 1$ -km-wide lava channel in southern Iceland (part of the Ögmundarhraun lava flow sequence on the Reykjanes Peninsula, Fig. 9a) is illustrated by means of a 30-cm horizontal resolution topographic profile in Fig. 9b (these data were collected by the AOL laser altimeter in a NASA P-3 aircraft). This channelized basaltic lava flow is extremely smooth at a variety of length scales (i.e., only 25-30 cm of topographic variance over baselines of hundreds of meters as indicated in Table 4) and represents a classic example of a low-viscosity Icelandic lava surface. The lava channel stands only about 6 m above an older flow surface. Figure 10 is a LOLA resolution profile of the perched lava channel that illustrates the 20-40-cm vertical roughness that



**Fig. 9.** (a) Airborne synthetic aperture radar (SAR) image of the Ögmundarhraun lava field in the Reykjanes region of southwestern Iceland. The radar look direction is from the south to the north at an average incidence angle of  $15^\circ$  from the horizon, and at X-band wavelength (data collected for NASA by INTERA Technologies using the STAR-2 system with 6-m resolution). This lava field consists of low-viscosity basaltic flows, many of which formed channels. The main lava channel in the center of the image displays well-defined levees, and an east-to-west cross-flow profile of this channel is shown below in (b). The Ögmundarhraun lava field was apparently emplaced about 700 years ago in a high volume eruption rate event (Garvin *et al.*, 1989). (b) Airborne laser topographic profile of a lava channel in the southern Reykjanes region (Ögmundarhraun) of Iceland acquired with a horizontal sampling interval of  $\sim 30$  cm by the AOL instrument in May 1987 (Hoge *et al.*, 1984). This smooth basaltic lava flow represents an analog to the smoothest lunar maria lavas and has an effective yield strength similar to that for Imbrium flows (Garvin *et al.*, 1989).

is characteristic of the flow interior, and the 2 m of topographic variance associated with the flow margins (levees). This profile extends from east to west across the long-axis of the flow direction (transverse profile). Low-viscosity lunar lava flows are inferred to behave much like this Icelandic basalt example on the basis of rheologic parameters estimated by Hulme (1975), Moore *et al.* (1978), and Hulme and Fielder (1977). Using the Moore *et al.* (1978) method as applied to profile in Fig. 10, we estimate the yield strength of the Icelandic flow to be on the order of 1300 Pascals (Garvin *et al.*, 1989). If lunar bases or science outposts were to be located in proximity to the most youthful

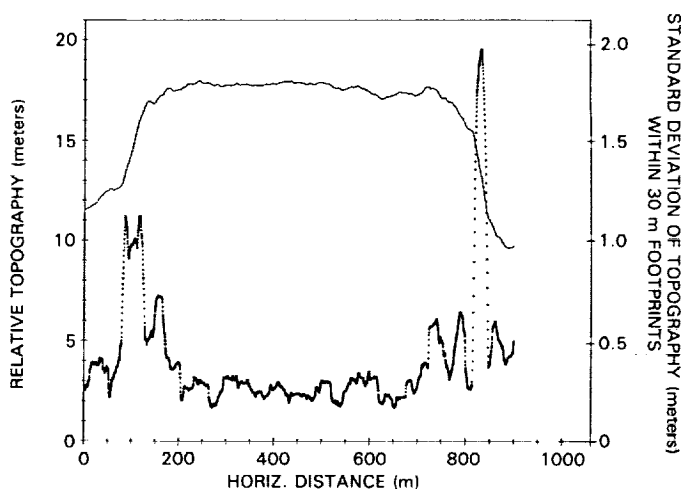


**Fig. 10.** The LOIA profile (as in Fig. 4) of the lava channel shown in Fig. 9b at 30-m horizontal sampling interval, with superimposed topographic variance parameter (dots). Observe the submeter scale roughness of this low-viscosity lava flow. Such surfaces could be common on the youngest lunar maria (H. J. Moore *et al.*, unpublished data, 1969).

low-viscosity lunar flows, perhaps to investigate their accessory mineral abundances (i.e., to measure Cr, Ni, Ti contents etc.), then examination of high-resolution topographic profiles may be useful in terms of identifying those flows with the least regolith development and hence the most pristine and accessible surfaces. Extremely smooth lava surfaces like that illustrated from southern Iceland are inferred to exist on the Moon, possibly associated with the freshest mare surfaces, but direct observation of their occurrence has not been possible. Lunar Observer Laser Altimeter topographic data could assist in the identification of the smoothest lunar surfaces in association with known volcanic features. Perhaps channelized lunar lava flows with submeter surface textures could be identified within Copernican-age surface units of suggested volcanic origin and evaluated as a possible lunar base site on the basis of synergistic laser altimeter data and high-resolution images.

Table 4 summarizes the anticipated range of within-footprint (on a 30-m baseline) vertical roughness as computed from the LOIA simulation profiles (and displayed as scaled standard deviation of topography on the figures). The most severe case would result in  $\sim 50$  m of dynamic range, with 20-30 m expected for the inner walls of fresh, simple impact craters. Smooth maria are likely to have anywhere from  $<1$  m to a few meters of vertical roughness, and for such surfaces, vertical precision of the LOLA measurements could approach the 15-cm lower limit. The potential ability of LOLA to detect locally rugged (as well as extremely smooth) topography will provide an important constraint in choosing lunar base location, especially for target areas not within the zone that was intensively surveyed for the Apollo site selection process (largely from stereo orbital high-resolution photography).

## SUMMARY

Analysis of laser altimeter profiles for representative lunar analog surfaces demonstrates that high spatial resolution topography of the lunar surface is a very desirable if not necessary

dataset for lunar base site selection and subsequent operations. A simple Observer-class instrument such as the Lunar Observer Laser Altimeter (LOLA) now under development as part of NASA's planetary program would be well suited for characterizing lunar topography and surface roughness at a variety of length scales appropriate for both addressing fundamental geoscience problems and local site selection and evaluation. A LOLA-class instrument would be ideally suited for operation in a low-altitude orbit around any body devoid of an atmosphere including the Moon, Mercury, or an asteroid.

Lunar base site selection will clearly involve complex decisions and tradeoffs on the basis of science potential, operational and safety factors, objectives, and types of precursory data that will be available. We suggest that laser topographic profiles and global topographic maps, together with orbital imaging (stereo, high-resolution, and multispectral) and Earth-based radar mapping will provide a necessary and sufficient framework from which to select optimal future lunar landing sites (e.g., for robotic rovers and astronauts) and eventually lunar base localities.

**Acknowledgments.** We are grateful for the assistance of M. T. Zuber and J. B. Abshire of NASA/GSFC in the preparation and review of this paper. We appreciate the support of NASA RTOP 157-03-80 from the PIDDP Program administered by L. Evans and W. Quaide. Support for the collection of airborne laser profiles using SLAP and AOL was kindly provided by NASA Geology Program RTOP 677-43-24; we thank the encouragement of P. Mougins-Mark and M. Baltuck in this effort. Pilots J. Riley, R. Gidge, V. Rabine, J. Hoag, and C. Allen, as well as flight mechanic C. Randall of the NASA's Wallops Flight Facility assured successful airborne laser profiling; the Sabreliner T-39 and P-3 aircraft were outstanding platforms from which to collect these data. Special thanks to chief data analyst M. Ford who reduced much of the airborne data collected to date, to L. Aist for performing the LGO orbital coverage simulations, to D. E. Smith for his encouragement, and to M. J. Cintala for his helpful editorial comments. Finally we thank the AOL team (R. Swift, W. Krabill, J. Youngel, and E. B. Frederick) for their enthusiastic assistance with Iceland data collection and analysis.

## REFERENCES

- Bufton J. L. (1989) Laser altimetry measurements from aircraft and spacecraft. *Proc. IEEE*, 77, 463-476.
- Bufton J. L. and Garvin J. B. (1987) Performance testing of the Shuttle Laser Altimeter. In *Proc. Optical Soc. Am. Topical Mtg. on Laser and Optical Remote Sensing*, pp. 13-16.
- Byer R. L. (1988) Diode laser-pumped solid state lasers. *Science*, 239, 742-747.
- Cintala M. J., Garvin J. B., and Wetzel S. J. (1982) The distribution of blocks around a fresh lunar mare crater (abstract). In *Lunar and Planetary Science XIII*, pp. 100-101. Lunar and Planetary Institute, Houston.
- Garvin J. B., Williams R. S., and Jónsson J. (1989) Geologic remote sensing of southwestern Iceland: An imaging radar and laser altimeter approach to problems in planetary volcanism. In *Proc. 28th Intl. Geol. Congress*, pp. 1-531 to 1-532. Washington, DC.
- Hoge F., Krabill W., and Swift R. (1984) The reflection of airborne UV laser pulses from the ocean. *Marine Geodesy*, 8, 313-344.
- Hood L., Sonnett C., and Russell C. (1985) The next generation geophysical investigation of the Moon. In *Lunar Bases and Space Activities of the 21st Century* (W. W. Mendell, ed.), pp. 253-264. Lunar and Planetary Institute, Houston.
- Hulme G. (1975) The interpretation of lava flow morphology. *Geophys. J. R. Astron. Soc.*, 39, 361-383.
- Hulme G. and Fielder G. (1977) Effusion rates and rheology of lunar lavas. *Philos. Trans. R. Soc. London*, A285, 227-234.
- Kaula W., Schubert G., Lingenfelter R., Sjogren W., and Wollenhaupt W. (1974) Apollo laser altimetry and inferences as to lunar structure. *Proc. Lunar Sci. Conf. 5th*, pp. 3049-3058.
- Long L. E., Ryan-Benoist R., and Konopelski T. W. (1989) Space-qualified diode-pumped slab laser. Paper given at SPIE, Los Angeles, California, January 1989. 7 pp.
- Moore H. J., Arthur D., and Schaber G. (1978) Yield strengths of flows on the Earth, Mars, and Moon. *Proc. Lunar Planet. Sci. Conf. 9th*, pp. 3351-3378.
- Moore H. J., Boyce J., Schaber G., and Scott D. (1980) Lunar remote sensing and measurements. *U.S. Geol. Surv. Prof. Pap. 1046-B*, pp. B1-B78.
- Phillips R. (1986) *Contributions of a Lunar Geoscience Observer to fundamental questions in lunar science*. LGO Science Working Group Members, Dept. Geol. Sci., SMU, Dallas. 86 pp.
- Ravine M. A. and Grieve R. A. F. (1986) An analysis of morphologic variation in simple lunar craters. *Proc. Lunar Planet. Sci. Conf. 17th*, in *J. Geophys. Res.*, 91, E75-E83.
- Sharpton V. and Head J. W. (1982) Stratigraphy and structural evolution of southern Mare Serenitatis: A reinterpretation based on Apollo Lunar Sounder Experiment data. *J. Geophys. Res.*, 87, 10,983-10,998.
- Shoemaker E. M. (1987) Meteor Crater, Arizona. *Geol. Soc. America Centennial Field Guide—Rocky Mountain Section*, pp. 399-404.
- Smith D. E., Zuber M., Garvin J., Bufton J., and Abshire J. (1989) The Mars Observer Laser Altimeter (MOLA) (abstract). In *Fourth Intl. Conf. on Mars*, Jan. 1989. Tucson, AZ, pp. 191-192.
- Wilhelms D. E. (1985) Unmanned spaceflights needed as scientific preparation for a manned lunar base. In *Lunar Bases and Space Activities of the 21st Century* (W. W. Mendell, ed.), pp. 245-252. Lunar and Planetary Institute, Houston.
- Wilhelms D. E. (1987) *The Geologic History of the Moon*. U.S. Geol. Surv. Prof. Pap. 1348. 302 pp.